CHAPTER 2

MODEL IDENTIFICATION STRATEGIES

2.1 Time domain and frequency domain identification

Various methods can be used to identify the natural frequencies present in the Experimental Fan Blade Damage Simulator (EFBDS). The simplest form would be to read the natural frequencies from a power spectral density, or similar frequency domain graph. Since the damage identification method need to be autonomous it was decided early on not to use a technique that depended on a certain amount of human expertise and experience which will certainly be required if a value has to be read of a graph prior to damage identification.

System identification is the field of modelling dynamic systems from experimental data. A schematic representation of a dynamic system can be seen if Figure 2.1. The system is driven by input variables u(t) and disturbances v(t). The user can control u(t) but not v(t). For the EFBDS the inputs are missing. The output signal originates from sensors such as accelerometers and dynamic strain gauges, designed to measure dynamic properties of the system.

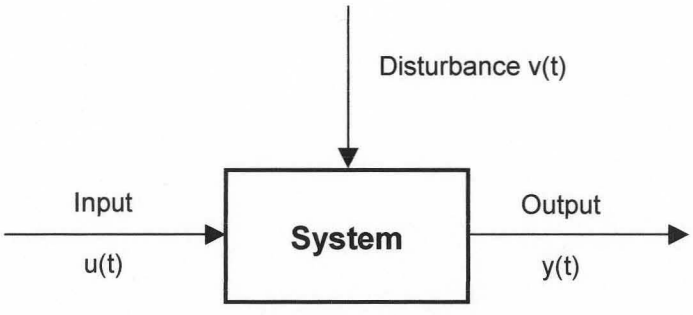

Figure 2.1 Typical example of a dynamic system

Mathematical models of systems are very useful in predicting behaviour of systems and although this is not necessary for this project, it will certainly be of paramount importance when automated detection using neural networks or similar methods are

implemented. Basically, there are two ways to model the EFBDS, mathematical modelling and system identification

- *Mathematical modelling:* This is an analytical approach. Basic laws from physics (such as aerodynamics, Newton's laws etc.) are used to describe the dynamic behaviour of the damage simulator.
- *System Identification:* This is an experimental approach. Some experiments are performed on the system; a model is then fitted to the recorded data by assigning suitable numerical values to its parameters.

Clearly it would have been very difficult to obtain an accurate mathematical model of this particular system due to the many stochastic external forces and complicated boundary conditions. A FEM was constructed that was, in essence, a mathematical model. More detail can be seen in the second part of this chapter.

Various modal identification techniques that require only output data were found in the literature study (Section 1.4). The problem with most of these techniques is that more than one output was required. While this was not an insurmountable problem (the data acquisition equipment used can sample up to four channels at the same time), the actual FD fan at the Majuba power generation fan has 20 blades. Even using one sensor per blade would already result in a huge amount of raw data, not to mention the cost involved (20 blades per fan, twelve fans at plant).

ARMA based curve fitting has been used by various researchers for the identification of modal parameters from output only data (see section 1.4). This algorithm was also readily available as a MATLAB toolbox. A brief description of this model is given below.

ARMAX model

The ARMAX model is short for an ARMA (AutoRegressive Moving Average) with an eXogenous signal (that is a control variable u(t)). A typical description of this model may be found in Torsten *et al. (1989)* and Pandit, (1991) .

Let *y(t)* and *u(t)* be scalar signals and consider the model structure:

$$A(q^{-1})y(t) = B(q^{-1})u(t) + C(q^{-1})e(t) \qquad \textbf{(2.1)}$$

where

$$A(q^{-1}) = 1 + a_1 q^{-1} + \ldots + a_{na} q^{-na}$$
$$B(q^{-1}) = 1 + b_1 q^{-1} + \ldots + b_{nb} q^{-nb} \quad \textbf{(2.2)}$$
$$C(q^{-1}) = 1 + c_1 q^{-1} + \ldots + c_{nc} q^{-nc}$$

The parameter vector is taken as

$$\theta = (a_1 \ \ldots \ a_{na} \quad b_1 \ \ldots \ b_{nb} \quad c_1 \ \ldots \ c_{nc})^T \quad \textbf{(2.3)}$$

The model (2.1) can be written explicitly as the difference equation

$$y(t) = a_1 y(t-1) + \ldots + a_{na} y(t-na) = b_1 u(t-1) + \ldots + b_{nb} u(t-nb) + e(t) + c_1 e(t-1) + \ldots + c_{nc} e(t-nc) \quad \textbf{(2.4)}$$

This model can easily be rewritten in state space format since from (2.1)

$$y(t) = \frac{B(q^{-1})}{A(q^{-1})} u(t) + \frac{C(q^{-1})}{A(q^{-1})} e(t) \quad \textbf{(2.5)}$$

For this structure (2.5),

$$G(q^{-1};\theta) = \frac{B(q^{-1})}{A(q^{-1})}$$
$$H(q^{-1};\theta) = \frac{C(q^{-1})}{A(q^{-1})} \quad \textbf{(2.6)}$$

There are several important special cases for (2.1)

- An autoregressive (AR) model is obtained when *nb*=*nc*=0. In this case a pure time series is modelled, no input signal is assumed to be present. In that case (2.1) reduce to

$$A(q^{-1})y(t) = e(t)$$
$$\theta = (a_1 \ \ldots \ a_{na})^T \quad \textbf{(2.7)}$$

- A moving average (MA) model is obtained when *na*=*nb*=0. Then

$$y(t) = C(q^{-1})e(t)$$
$$\theta = (c_1 \quad \ldots \quad c_{nc})^T \tag{2.8}$$

- An autoregressive moving average (ARMA) model is obtained when *nb*=0. Then

$$A(q^{-1})y(t) = C(q^{-1})e(t)$$
$$\theta = (b_1 \quad \ldots \quad b_{nb})^T \tag{2.9}$$

- Another special case is when *nc*=0. The model structure then becomes

$$A(q^{-1})y(t) = B(q^{-1})u(t) + e(t)$$
$$\theta = (a_1 \quad \ldots \quad a_{na} \quad b_1 \quad \ldots \quad b_{nb})^T \tag{2.10}$$

This is sometimes called an ARX (controlled autoregressive) model.

The AR and ARMAX (reduced to an ARMA model because of the output only data) subroutines were the only models that could be used in the system identification toolbox of MATLAB. The AR model was substantially less expensive computationally but the ARMAX model outperformed the later in terms of accuracy and was chosen instead. Appendix C reviews initial studies done to establish the constraints of the ARMAX model.

2.2 Finite Element Modelling

As described in Chapter 1, the forward frequency problem was often solved with the help of mathematical models of the physical system. Since it is known that only limited success was achieved when frequency shifts has been used to detect damage, it was decided to create a mathematical model to ascertain the viability of using this technique.

Finite element modelling has become a widely used tool in the field of vibration monitoring and damage detection. Various papers make use of FEM only to test damage identification techniques (see Chapter 1). It soon became apparent that the

number of elements used in the mesh, aspect ratio of the elements and element type used, made a substantial difference to the mode shapes corresponding natural frequency. A study to determine the mesh refinement and element type that should be used was therefore undertaken.

2.2.1 Mesh refinement

In order to determine the required mesh refinement to produce accurate results, a simple beam was constructed. In this way the exact natural frequencies could be computed numerically. A summary of the analytical and finite element model results for different meshes and elements can be seen in Table 2.1. The natural frequencies could be analytically calculated as follows:

For free vibration of a uniform beam, the natural frequencies are given by

$$f_n = A_f \sqrt{\frac{EI}{\rho A L^4}} \qquad \textbf{(2.11)}$$

The A_f value change with different boundary conditions. These values were found in Barber (1992).

The methodology to find an analytical formulation such as equation 2.11 can be found in a number of literature sources, Rao (1995) provides a good example.

Interestingly enough, it was not possible to obtain accurate results using first order, 8 node brick elements. Even when a refined, dense mesh was used, the natural frequencies calculated still differed by as much as 15% from the analytically calculated frequencies. The situation deteriorated the higher the natural frequency was. This phenomenon was caused by the inherent stiffness of a first order element. The complex shapes of the actual blades made the use of solid elements desirable. These elements also make the construction of a model simpler.

Results for different mesh refinements and element types can be seen in Tables 2.1 and 2.2. Only in-plane modes were analysed (horizontal and vertical in Figure 2.2).

Basically the 8-node element uses a constant strain integration scheme through the element which causes this element to perform poorly in bending. Since most mode shapes show extensive bending in the vertical or horizontal plane, this made a huge difference when calculating the natural frequencies.

A second order 20-node brick element with mid-side nodes was tested next. This element assumes a linear distribution of strain throughout the element. This allows for an accurate representation of the strain fields in elastic analysis. As a result this element gives almost exact predictions of natural frequencies. Furthermore 27-point Gaussian integration is used for the stiffness calculation, compared to the 8-point Gaussian integration used with the 8-node element.

The reason why the horizontal natural frequencies (see Figure 2.2) were predicted much more accurately with 8-node brick element than the vertical natural frequencies, can be explained as follows: Only about a fifth the amount of beams used through the horizontal cut of the beam were used through the vertical cut. In essence the mesh was more refined in the horizontal direction and it is known that the accuracy of the 8-node beam element increased when the mesh was refined (see Table 2.2).

Table 2.1: Comparison of natural frequencies found for 1m aluminium hinged beam.

Vertical natural frequencies				
Description	**Mode 1**	**Mode 2**	**Mode 3**	**Mode 4**
Analytical values	8.23	52.4	144.3	283.1
8-node, course mesh (760 elements)	13.7	96.9	279.7	551.1
8-node, very fine mesh (4400 elements)	11.3	74.6	211.2	414.8
8-node, good aspect ratio (2000 elements)	8.98	56.2	157.4	308.1
20-node, course mesh (760 elements)	8.23	51.8	144.3	284.6

Table 2.2: Comparison of natural frequencies found for 1m aluminium hinged beam.

Horizontal natural frequencies				
Description	**Mode 1**	**Mode 2**	**Mode 3**	**Mode 4**
Analytical values	74.1	472	1299	2548
8-node, course mesh (760 elements)	70.4	425	1127	2277
8-node, very fine mesh (4400 elements)	70.3	425	1128	2300
8-node, good aspect ratio (2000 elements)	74.0	447	1189	2370
20-node, course mesh (760 elements)	74.1	447	1190	2400

Clearly, it was also of paramount importance that a good aspect ratio was used throughout. Even though a very fine mesh of 4400 elements was used at one stage, a mesh with only half that number of elements gave much closer results to the analytical solution because the aspect ratio was kept within the guidelines of good meshing. The quadratic element was not effected as much by a bad aspect ratio because of the linear distribution of strain used for this element.

A graphical presentation of Table 2.1 and 2.2 can be seen in Figures 2.3 and 2.4 respectively. Clearly a FEM can give grossly inaccurate results if meshing and element choice are not done with care. Predicted natural frequencies were in error by up to 90% when a coarse mesh with a bad aspect ratio was used. This was largely due to the linear strain distribution used for an eight-node brick element. Very accurate predictions regarding natural frequencies could be made even when a coarse mesh with a bad aspect ratio was used and the quadratic element was used.

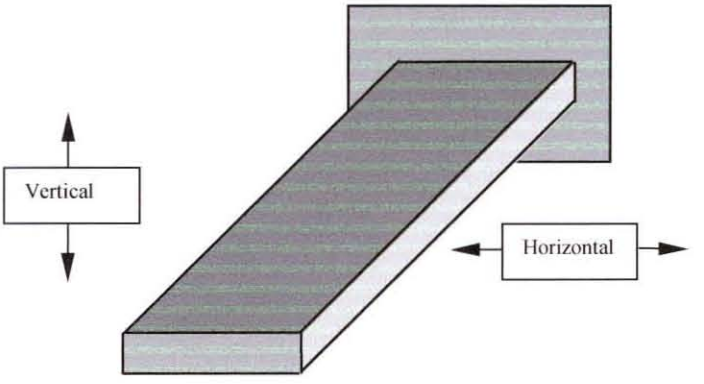

Figure 2.2: Schematic representation of test beam used for FEM testing

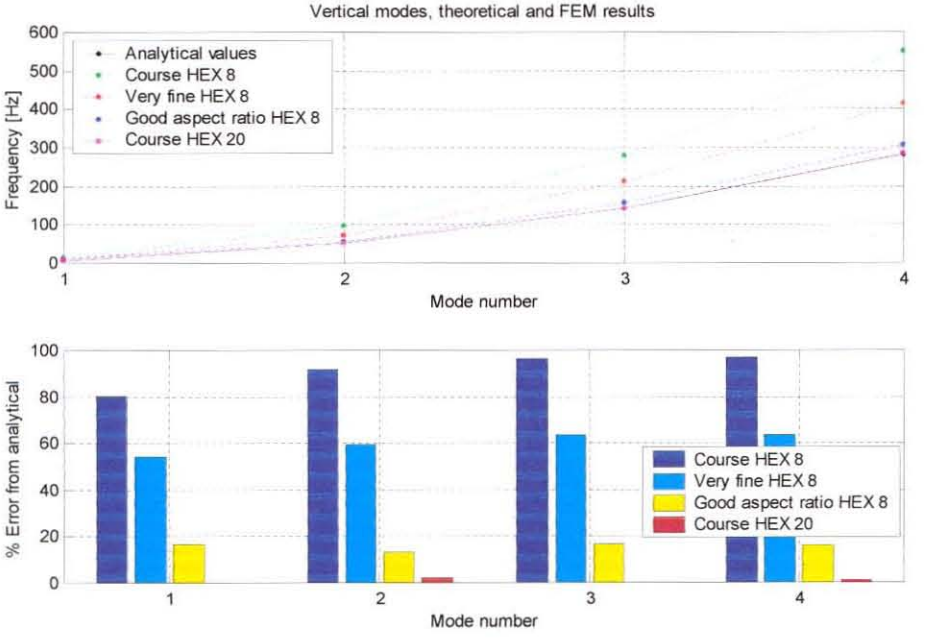

Figure 2.3: Graphical presentation of Table 2.1

The 20-node brick element was substantially more expensive computationally. This was because of the triquadratic interpolation used by the second order element together with the 27 point Gaussian integration for the stiffness of the element. The 8-node brick element use trilinear interpolation functions and 8-point Gaussian integration. In order to get the same accuracy for the mode shape frequencies, the mesh had to be so much refined that computational time actually became unacceptably high and the analysis was stopped before completion.

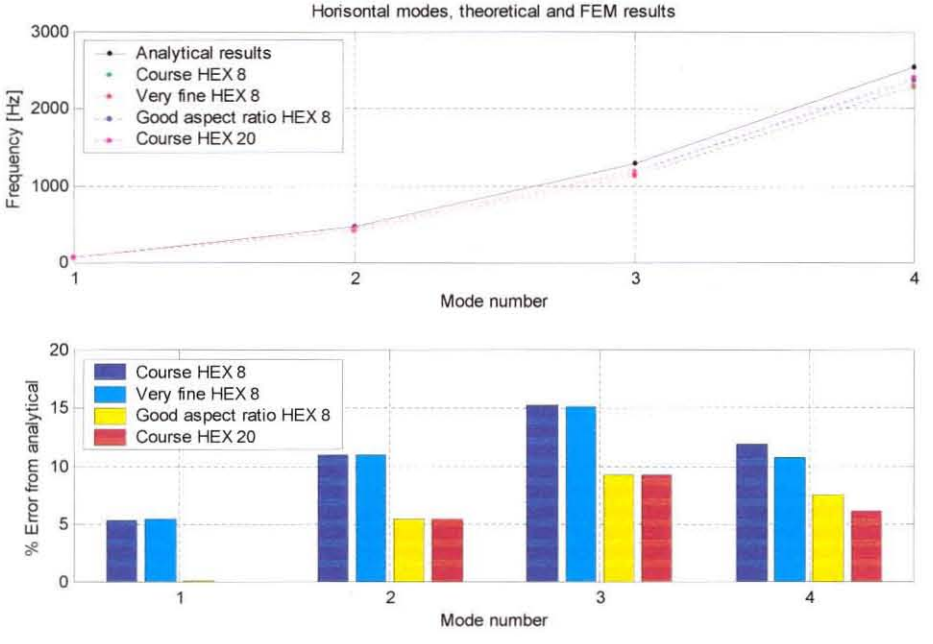

Figure 2.4: Graphical representation of Table 2.2

2.2.2 Modelling of experimental fan blade damage simulator

After guidelines for the accurate modelling of blade like structures had been established, a model of one blade of the experimental fan blade damage simulator was constructed. An important difference between the stationary beams analysed in the previous section and a fan blade, is the centrifugal acceleration imposed on the blade. Fortunately, modern Finite Element (FE) software allows these boundary conditions to be added with relative ease. For accurate results it is however, necessary to use load steps since an iterative approach to finding the updated stiffness matrix for a centrifugal load is used by most software. Five consecutive analyses were therefore performed starting at one fifth the rotational velocity.

As a first attempt, a very simple clamped beam with the same dimension as the actual blade was modelled. Natural frequencies found by means of the FEM are compared to the frequencies found experimentally in Table 2.3. The fifth mode shape can be seen in Figure 2.5.

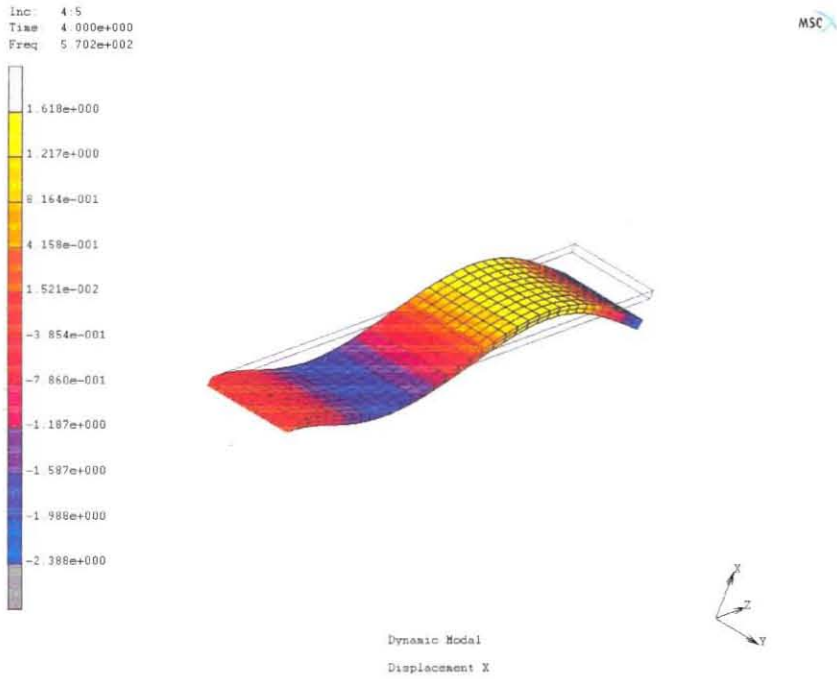

Figure 2.5: Simple FEM used as first iteration.

Table 2.3: First FEM results compared to experimental results.

Mode number	FEM value	Experimental value
1	36.63	33.41
2	205.4	203.3
3	319.6	285.5
4	441.9	447.3
5	572.9	563.5

While reasonable accuracy was obtained, even better overall results were found when the FEM was slightly modified to more accurately resemble the experimental fan blade damage simulator. An example of this model can be seen if Figure 2.6. Results for the natural frequencies found can be seen in Table 2.4.

The purple areas at the base of the blade in Figure 2.6, represent the boundary constraints that was imposed. These nodes were constrained in the x, y and z directions. The experimental and FEM results can be seen in Table 2.4

Table 2.4: More accurate FEM results compared to experimental results.

Mode number	FEM value	Experimental value
1	34.53	33.41
2	202.4	203.3
3	285.2	285.5
4	435.1	447.3
5	562.8	563.5

Fig 2.6: More accurate FEM for fan blade damage simulator.

While some difference still existed between the finite element model and the experimentally obtained results, the prediction was fairly good overall. The results obtained in all Finite Element Analyses (FEA) were at 750 r.p.m. as were the results obtained during experimental measurements. The reason for the inaccuracy of the fourth (first torsional) mode shape were the inconsistency of welds found in the EFBDS. Figure 2.7 shows a close up of the root of the blades used in the EFBDS.

The next step was to introduce artificial damage to the finite element model that would be representative of the damage induced on the EFBDS.

2.2.3 Damage modelling using FEM

During recent years finite element modelling has become a very attractive method for simulating real life systems. This is mostly due to the fact that very fast, relatively inexpensive desktop computers can now be used to run the packages. MSC Marc can for example model the very complicated behaviour of fatigue cracking. While

these modelling tools can never replace experimental measurements and do not give exact answers, it can save a substantial amount of time and money.

In this specific case, the object was not to compute the exact stress concentration and fatigue life of the blade. If this could be done with any degree of accuracy, a monitoring technique would not be necessary, provided no external influences that could damage the blade (such as debris) are present. Due to the nature of the damage induced by a fine hack saw (see Figure 2.7) stress concentration factors and other fatigue information for the material are not required. This method of inducing damage does provide near crack like behaviour for the dynamics of the system (Cawley and Ray 1988). Basically there are three methods with which the damage done to the EFBDS can be modelled:

- Nodes can be untied from each other on the cut surface.
- The modulus of elasticity can be decreased in the neighbouring elements
- Elements can be removed. This requires a very fine mesh however and is not a practical option.

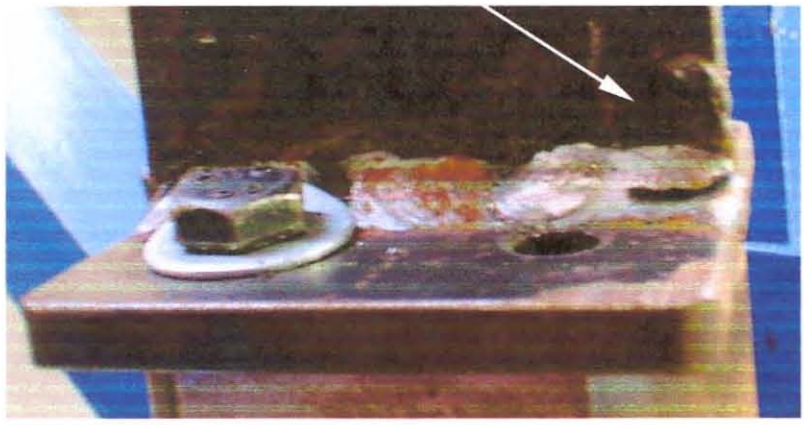

Figure 2.7: 15% Damage inflicted by using a fine hack saw.

The first two options provided simple and effective solutions to the problem. Since the actual damage induced on the EFBDS consisted of using a fine hacksaw to saw through part of the blade at the root, disconnecting the nodes provided an accurate representation of the damage. The exaggerated movement of the FEM model can be seen in Figure 2.8. Disconnecting the nodes allow the faces to move through each other. While it did not model an actual crack well, it was an accurate depiction of EFBDS.

When the modulus of elasticity was adjusted for damage it was found that although the model could be optimised to give very close to the same results as were found

experimentally, the general trend with increasing damage was substantially worse. For the case of modelling an opening and closing crack, this method could work very well since a non-linear modulus of elasticity with a normal modulus in the closing direction and a reduced modulus in the opening direction could be used.

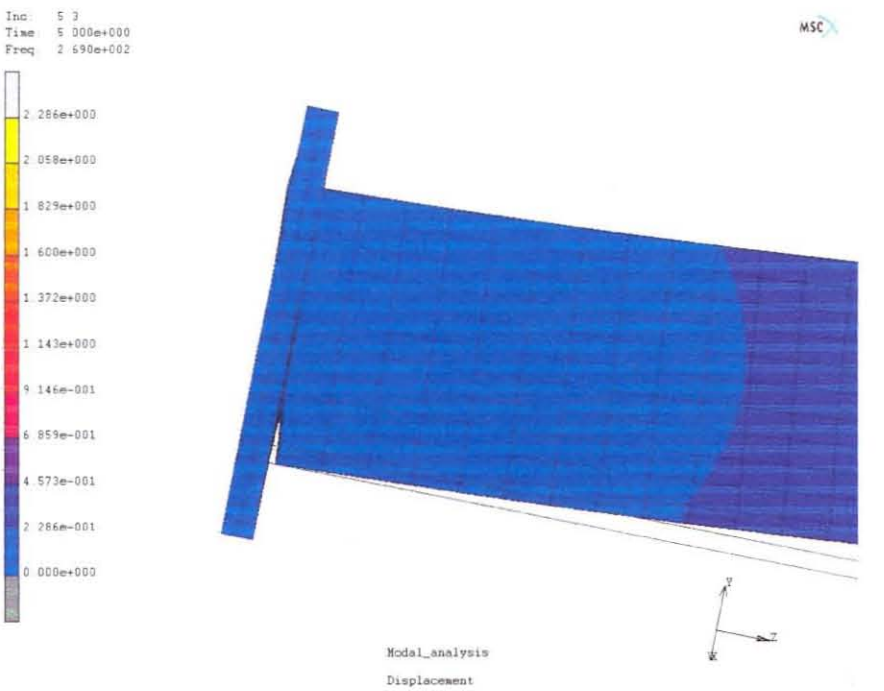

Figure 2.8: Exaggerated movement of FEM model with a 30% crack.

When the model was optimised as far as possible to give results very close to the undamaged experimental frequencies found, nodes were untied and modal extraction performed. The results for various damage levels are shown in Figure 2.9.

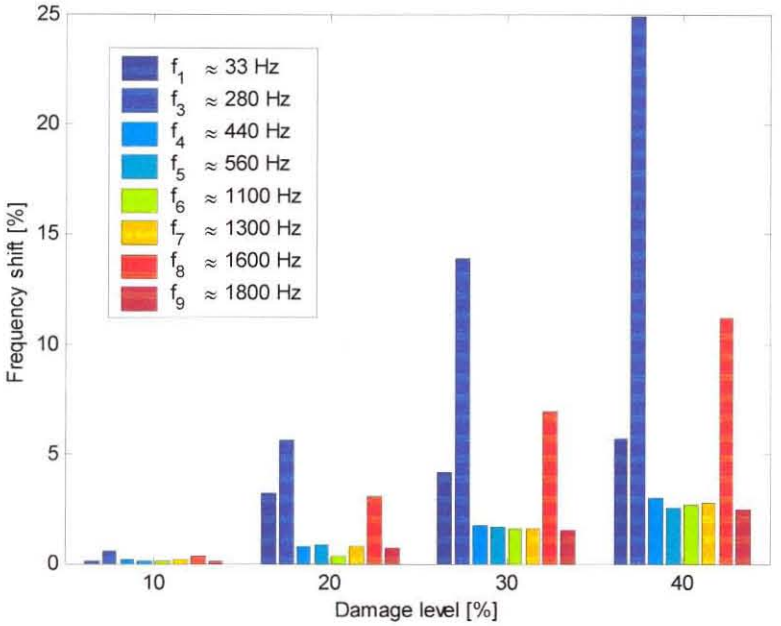

Figure 2.9: FEM results for increasing damage levels at different natural frequencies.

As can be expected, the shift showed an exponential trend as more damage was induced. Although the first frequency seemed to be a relatively good choice, it had to be remembered that a frequency shift of 2.5% means that the frequency change from around 34.5 Hz, to 33.6 Hz. Due to electrical noise, drift and other external influences some measurement error can be expected. Furthermore the resolution with which frequencies were measured was generally about 0.33 Hz due to the discrete nature of peak picking algorithms. This represents a 1% error at 34 Hz but only 0.1% at 280 Hz. The obvious frequency to use would be the one found at 280 Hz.

The second natural frequency showed very little promise as a damage indicator and was not used at all. This turned out to be the case for the EFBDS as well. The experimental results can be seen in Chapter 4.

2.2.4 Results for curved blade

For various reasons described in Chapter 1, it was decided to use an EFBDS to develop a damage detection method. Since this project may be expanded to include the FD and ID fans found at the Majuba power plant, it was decided that a FEM would be used to show that the techniques used for a simple blade on the EFBDS also apply to more complex curved blades which is found more often in practice.

A single blade with very close to the same dimensions as that found on an actual blade on a FD fan was modelled using MSC MARC. The boundary constraints used for this model can be seen in Figure 2.10.

Figure 2.10: Boundary conditions (purple) for the FEM of the FD-fan blade.

The crack can propagate from the trailing edge of the blade or from the leading edge. Both these scenarios were modelled using suitable FEM models. While the computer time for the simple T-blade given in the previous section was typically seven minutes, the curved blade took around 70 minutes. The results for the trailing edge crack can be seen in Table 2.5 and the leading edge in Table 2.6. The reason for choosing 16%, 23% and 33% for the trailing edge and 12%, 21% and 31% for the leading edge is the discrete nature of the FEM. Since nodes were untied to simulate damage and the airfoil section is not symmetrical, different areas are effectively damaged.

Table 2.5: Frequency shifts due to trailing edge cracks.

Mode number	0% damage	16% damage	23% damage	33% damage
1	23.67	23.35	23.17	22.92
2	100.7	96.94	91.49	81.49
3	111.1	106.8	104.1	101.3
4	141.3	140.5	140.1	139.9
5	262.4	259.6	258.7	256.8
6	409.8	407.6	405.8	402.3
7	492.9	488.1	485.8	482.0
8	666.0	652.8	639.8	619.6
9	697.1	691.7	686.9	678.6
10	783.2	777.4	774.3	767.2
11	982.2	975.9	969.9	957.6

Table 2.6: Frequency shifts due to leading edge cracks.

Mode number	0% damage	12% damage	21% damage	31% damage
1	23.67	23.51	23.28	22.86
2	100.7	100.2	99.0	90.64
3	111.1	108.1	103.0	98.83
4	141.3	140.4	139.2	136.7
5	262.4	260.5	258.0	254.7
6	409.8	408.2	405.4	399.9
7	492.9	490.4	487.1	481.6
8	666.0	658.1	646.4	625.3
9	697.1	693.8	688.2	677.9
10	783.2	779.7	775.8	770.0
11	982.2	977.8	970.9	957.0

A comparison of the crack locations can be seen in Figure 2.11.

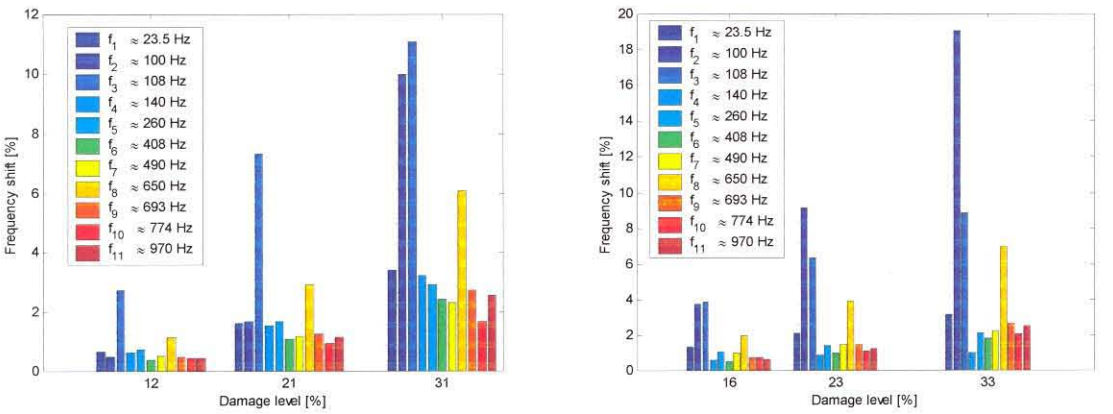

Figure 2.11: The leading edge can be seen on the left while the trailing edge van be seen on the right.

Again, some of the modes were more susceptible to damage than others. The obvious choices here would be the second, third or eighth mode shapes. The accuracy with which the various mode shapes can be measured and the potentially global nature of some of the mode shapes will make it necessary to create a more detailed finite element in conjunction with preliminary measurements on the actual blades to determine the accuracy of the FEM model.

Some of the mode shapes found during the FEA can be seen in Figures 2.12 and 2.13. Because of the airfoil cross-section of the blade, it was not easy to intuitively decide what shapes would be found. The placement of sensors for optimal sensitivity with regard to two or more mode shapes could be done by studying these findings. Chapter 5 deals with the phenomenon of global and local mode shapes.

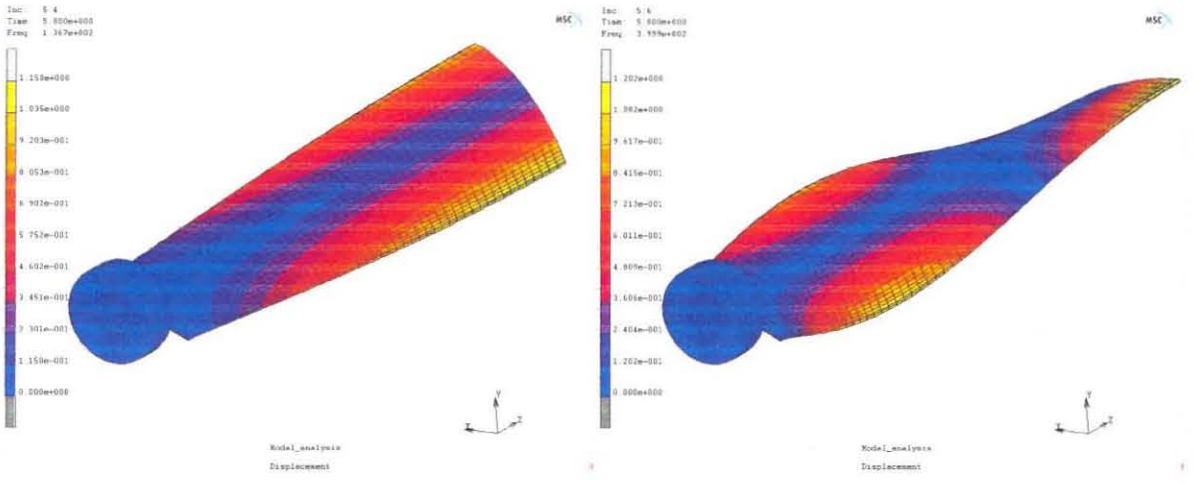

Figure 2.12: The fourth (left) and sixth (right) mode shapes for a curved blade.

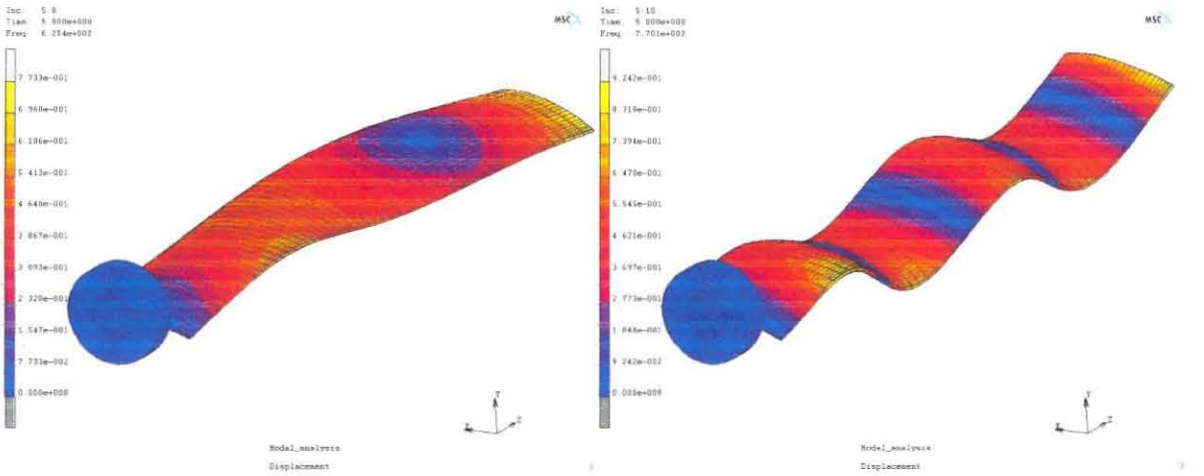

Figure 2.13: The eighth (left) and tenth (right) mode shape for a curved blade.

The contour bands in Figure 2.12 and 2.13 represent scalar displacement of the blade. These displacement plots could be used to determine the optimal location for the placement of accelerometers. This was not necessary for the simple blade used by the EFBDS since both the mode shapes used (first sideways, Figure 2.8 and first torsional) for damage level detection caused maximum strain and movement at the same location. If a high number of frequencies are to be used however, this situation may change and an optimal location can then be found by mathematical optimisation.

2.3 Conclusion

A model identification strategy that would provide modal parameters (natural frequencies) was selected in this chapter. Furthermore a FEM of the fan blade damage simulator used to develop a damage detection technique for fan blades was developed. FEA showed that the frequency shifts due to simulated damage should be significant enough to detect using natural frequencies only as a damage indicator.

It was also found that FEM packages such as MSC MARC gave very good correlation with both analytical results and experimental results. A model that closely resembles the blades found on the FD fan at the Majuba power generation plant was also developed. This model showed similar trends regarding frequency shifts with increasing levels of damage. The following were the most interesting:

- Although the asymmetric nature of the airfoil section does not lend itself to a sideways mode shape, the nearest comparable mode shape was also very sensitive to damage.
- Sensitivity differed depending on whether the crack was introduced on the leading or trailing edge, this could complicate experimental classification of damage.
- Because the actual FD blades are physically larger than the EFBDS blades, the natural frequencies are a lot lower. This implies that a lower sampling frequency can be used. A lower sampling frequency means less data needs to be processed and lower order ARMAX models can be used.

Provided good experimental results could be found, there was every reason to believe that a damage detection technique for fan blades could be developed both for the EFBDS and actual fan blades in industry.